Increasing the PV hosting Capacity of Distribution Grids with Distributed Storage: Siting, Sizing and Costs

Fabrizio Sossan, Rahul K. Gupta, Enrica Scolari and Mario Paolone
Distributed Electrical Systems Laboratory (DESL), Swiss Federal Institute of Technology of Lausanne (EPFL)

September 3, 2018

Executive Summary

The capacity of electrical distribution systems of hosting photo-voltaic (PV) generation is limited due to the requirements of distribution system operators (DSOs) to respect statutory voltage levels along feeders and not exceed line current limits. Traditional ways to perform voltage regulation in distribution systems are on-load tap changers, voltage series regulators, and coordinated control of the reactive power set-points of PV converters, that however is ineffective in low voltage distribution systems due to the large R/X ratio of the longitudinal parameters of lines. The problem of line current congestions is normally tackled by curtailing PV generation, a practice that is however inefficient because it decreases the capacity factor of PV plants. Thanks to their decreasing cost, battery energy storage systems are gaining of interest as they can provide both voltage control and congestion management, avoiding the use of multiple countermeasures among those listed above. Distributed battery energy storage systems for grid control could be owned and operated by distribution system operators directly, and become a new safeguarding asset for grids. The battery fleet and control infrastructure can be designed to meet industrial-grade operational standards for control accuracy, reliability, and maintenance. This feature would not be possible with behind-the-meter PV self-consumption equipment installed by end customers (which can also relieve grid congestions by promoting the consumption of locally generated electricity) because this asset would not belong to the operator.

In this report, we describe a method to plan the deployment of grid-connected batteries in distribution systems with the objective of accommodating a target level of PV generation capacity. The method determines the location, energy capacity and power rating of the batteries with the minimum capital costs such that their injections can restore suitable nodal voltages and line currents in the network. The method is tractable thanks to leveraging an exact convex formulation of the optimal power flow problem and a convex battery model that includes the notion of charging/discharging efficiency. We apply the method to a low voltage (LV) and medium voltage (MV) distribution network, modeled according to the specifications of the CIGRE's benchmark systems.

The analysis is carried out for different levels of installed distributed PV generation capacity, from zero up to 3 times the generation hosting capacity of the grid. Uniform clear-sky conditions are considered as they are conducive to the largest yield from distributed PV generation. In the considered case studies, it is shown that for very large values of PV penetration levels (i.e., twice the PV hosting capacity), the total power rating of the deployed battery systems grows in a 1-to-1 ratio with the installed PV capacity. For less extreme values of installed PV capacity, the growth is generally smaller. The total energy capacity of batteries grows faster than for the power rating due to the typical peak production patterns of PV generation, that typically occur in the middle of the day and last for several hours. In particular, once the injection from a PV plant determines an over-current or over-voltage, it needs to be postponed and stored until it persists (e.g., hours), thus determining large energy capacity requirements. Using distributed battery storage to

Research supported by the "joint activities on scenarios and modelling" program of the Swiss competence center on energy research (SCCER-JASM)

mitigate grid congestions caused by distributed PV generation is an energy-intensive application that can be coupled with power-intensive applications, like primary frequency regulation, by leveraging algorithms for the provision of multiple ancillary services.

1 Methods

It is given an electrical distribution network interfacing prosumers (i.e., demand and distributed PV generation) to the upper grid level. We consider a radial system, that is the typical way of interfacing consumers in low voltage (LV) and medium voltage (MV) distribution systems. The objective of this work is to determine the location, power rating and energy capacity of batteries at the lowest capital investment cost to accommodate a target level of PV generation such that it does not cause violations of electrical networks constraints, i.e., respecting statutory voltage limits along the feeders and line currents. The problem is formulated as a constrained optimization problem, which is introduced in the following in its various parts.

Cost function The expression to minimize is the capital investment cost, that is modelled as the sum between the cost of energy capacity, cost of apparent power rating and cost of grid connection. Let $n = 1, \dots, N$ be the index of the potential battery locations (or electrical bus), $\bar{E}_n$ the energy capacity of the battery at location n, $\bar{S}_n$ the apparent power rating of the power converter at location n, and u_n a flag denoting the presence of the battery at location n:

$$u_n(\bar{S}_n) = \begin{cases} 1, \text{ if } \bar{S}_n > 0 \\ 0, \text{ otherwise} \end{cases} . \tag{1}$$

Then, the investment cost is:

$$c(\bar{E}_1, \dots, \bar{E}_N, \bar{S}_1, \dots, \bar{S}_N) = \sum_{n=1}^{N} \left(c_E \cdot \bar{E}_n + c_S \cdot \bar{S}_n + c_G \cdot u_n(\bar{S}_n) \right) \tag{2}$$

where c_E, c_S and c_G are input parameters and denote the unitary price of power, energy and grid connection in USD/kVA, USD/kWh, and USD, respectively.

Electrical grid model The electrical grid model determines nodal voltages and line currents as function of the grid topology, characteristics of cables, and nodal injections. It is used to impose grid operational constraints. AC load flow equations are notoriously nonlinear and, when included in optimization problems, originate non convexity. In this work, we use an exact convex formulation of the AC optimal power flow problem from the literature, called augmented relaxed optimal power flow (AR-OPF) [1]. Compared to alternative methods, AR-OPF includes in the formulation the notion of transverse parameters and introduces a new set of conservative constraints to assure the feasibility of the solution. In this paragraph, the description is limited to introducing a general notation for the optimal power flow problem, while details and formal proofs about the convex equivalency can be found in Appendix A and in [1].

Let $n = 1, \dots, N$ denote the electrical bus of the network, $t = 1, \dots, T$ the time index, v_{tn} the voltage magnitude at time t and bus n in per unit (pu), $l = 1, \dots, L$ the index of the electrical line, i_{tl} the line current magnitude at time t in line l in pu, and R_{tn} the time variant apparent power nodal injection at time t and bus n in kVA. The electrical grid model implemented in the optimization problem is, for each instant of time t:

$$f(\widetilde{v}_{t1}, \dots, \widetilde{v}_{tN}, \widetilde{i}_{t1}, \dots, \widetilde{i}_{tL}, \widetilde{v}_{t0}, R_{tn}, \dots, R_{tN}) = 0 \tag{3}$$

$$v_{\min} \leq v_{tn}(P, Qoverspace) \leq v_{\max} \tag{4}$$

$$|i_{tl}| \leq \bar{i}_l \tag{5}$$

where (3) denotes the load flow model, the symbol $\sim$ denotes phasors, v_{t0} is the voltage at the grid connection point, the couple $v_{\min}, v_{\max}$ defines the bounds of the allowed voltage limits, and $\bar{i}_l$ is the line ampacity limit.

The apparent nodal injection at the nodes is denoted by R_{tn} and consists of apparent prosumption (i.e., conventional noncontrollable demand and PV generation), denoted by D_{tn}, and battery active and reactive demand, denoted by P_{tn} and Q_{tn}, respectively. The apparent nodal injection is:

$$R_{tn}\left(P_{tn}, Q_{tn}\right) = D_{tn} + P_{tn} + jQ_{tn}. \tag{6}$$

The prosumption profiles are an input to the problem and are from measurements, as specified in the description of the case study later, whereas the battery demand is a variable and an output of the optimization problem.

Battery energy system model Battery systems and their constraints are modelled in terms of their converter power rating and energy capacity. Batteries are grid-connected with conventional four-quadrant converters with a circular PQ characteristic, with radius as the converter's apparent power rating. To model battery energy constraints and losses of the charging/discharging process, we use the approach proposed in [2] that models lumped losses in the transformer, power converter and cell stack during charges and discharges with a Thevenin equivalent circuit (i.e. an ideal voltage source with a series resistance) estimated from measurements. The additional circuitry, shown in Fig. 1 is added in series to the nodes equipped with batteries, allowing for a seamless integration of the notion of storage's charging/discharging efficiency in the load flow problem. This approach is more accurate than the constant efficiency model, e.g. [3], since losses of batteries are normally proportional to their charge/discharge rate. As we use a convex formulation of the AC OPF problem, the additional nodes for the batteries do not impact on considerations about convexity. Additional battery's nodes in the grid are a modelling abstraction, and no grid constraints for those portions of the network are enforced.

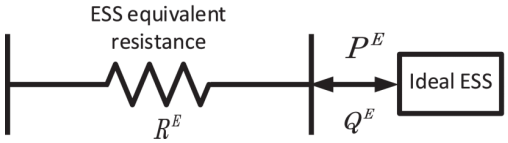

Figure 1: ESS model.

Let ΔT denote the sampling time in seconds, E_{tn} the state of energy at time t of the battery at node n in kWh, P_{tn} the battery active power demand in kW, Q_{tn} the power converter reactive power in kVAR, and L_{tn} the battery resistive losses in kW. The evolution in time of the state of energy of batteries is:

$$E_{tn}(P_{tn}) = E_{(t-1),n} + (P_{tn} - L_{tn})\Delta T/3600. \tag{7}$$

Batteries' operational constraints concern respecting the physical limits of the state of energy and power converter rating. They are:

$$0 + \epsilon_n^- \leq E_{tn}(P_{tn}) \leq \bar{E}_n - \epsilon_n^+ \tag{8}$$

$$P_{tn}^2 + Q_{tn}^2 \leq \bar{S}_n^2, \tag{9}$$

where ϵ_n^- and ϵ_n^+ are arbitrary back-off terms to implement conservative energy bounds. Aging phenomenon could be accounted for by limiting the energy exchange of the battery, as for example developed in [4].

Problem formulation The optimization problem determines the values of energy capacity and power rating at the various locations by minimizing the capital investment cost subject to batteries' and grid's operational constraints. For convenience in the following development, we group the values of batteries' energy capacity and power rating in the vectors $\bar{\boldsymbol{E}} = [\bar{E}_1, \ldots, \bar{E}_N]$ and $\bar{\boldsymbol{P}} = [\bar{P}_1, \ldots, \bar{P}_N]$, batteries' active

power and reactive power in the $\boldsymbol{P} = [P_{1n}, \ldots, P_{T1}, P_{12}, \ldots, P_{TN}]$ (i.e., stacking the time and bus dimensions) and $\boldsymbol{Q} = [Q_{1n}, \ldots, Q_{T1}, Q_{12}, \ldots, Q_{TN}]$. For the last two vectors, if they are indexed, then only dimension not reported in the index is stacked, e.g. $\boldsymbol{P}_t = [P_{t1}, \ldots, P_{tN}]$. The problem formulation is:

$$\underset{\bar{\boldsymbol{E}}, \bar{\boldsymbol{S}}, \boldsymbol{P}, \boldsymbol{Q}}{\text{minimize}}\, c\left(\bar{\boldsymbol{E}}, \bar{\boldsymbol{S}}\right) \tag{10}$$

subject to grid's and batteries' operational constraints

$$v_{\min} \leq v_{tn}(\boldsymbol{P}_t, \boldsymbol{Q}_t) \leq v_{\max} \qquad \text{for each } t \text{ and } n \tag{11}$$
$$|i_{tl}| \leq \bar{i}_l \qquad \text{for each } t \text{ and } l \tag{12}$$
$$0 + \epsilon_n^- \leq E_{tn}(\boldsymbol{P}_n) \leq \bar{E}_n - \epsilon_n^+ \qquad \text{for each } t \text{ and } n \tag{13}$$
$$P_{tn}^2 + Q_{tn}^2 \leq \bar{S}_n^2 \qquad \text{for each } t \text{ and } n, \tag{14}$$

and grid's and batteries' models

$$f(\widetilde{\boldsymbol{v}}_t, \widetilde{\boldsymbol{i}}_t, \widetilde{v}_{t0}, \boldsymbol{R}_t(\boldsymbol{P}_t, \boldsymbol{Q}_t)) = 0 \qquad \text{for each } t \tag{15}$$
$$E_{tn}(\boldsymbol{P}_n) = E_{(t-1),n} + (P_{tn} - L_{tn})\Delta T/3600 \qquad \text{for each } t \text{ and } n. \tag{16}$$

t In other words, the batteries' injections are slack variables of an optimal power flow problem, which are adjusted to correct potential violations of nodal voltages and line currents limits while subject to battery models.

2 Case study and simulated scenarios

Case study To reflect the two mainstream trends for deployment of PV generation, we consider two grid configurations: a MV and a LV distribution system. The former is typical for industrial and utility-scale PV production facilities, whereas the latter represents the case of small rooftop commercial and domestic PV plants. Grids are modelled according to the Cigre' specifications for the European grid benchmarks for MV and LV distribution systems described in [5] and shown in figures 4b and 4a, respectively. The MV grid is a 14 nodes 20 kV/25 MVA, and the LV grid is a 18 nodes 0.4 kV/400 kVA, both three-phase. In this analysis, they are considered in terms of their single phase equivalent. The nominal values of commercial and domestic demand along with the PV capacity in the base case is reported in Table 1. The base case approximates the PV hosting capacity of the respective network. It is calculated with the algorithm described in [6] by determining the maximum level of PV generation that the grid can host without violating network constraints and subject to preferred locations for PV plants (i.e., nodes with demand and close to the grid connection point), land use limits and physical constraints[1]. The total PV installed capacity in the base case is approximately 41 MW in the MV grid and 0.52 MW in the LV, whereas the nominal demand is 46 MVA and 0.4 kVA, respectively. Considering the PV production pattern of the clear-sky day of Fig.3 (that is with 0.31 pu average power on a 1-day period) and average daily consumption of 0.4 pu, the LV network approximates a net-zero-energy system, whereas the daily energy balance of the MV network requires to import electricity from the upper grid layer.

For the LV network, we assume that not all locations can host batteries due to, e.g., land use constraints. Available nodes are 1, 11, 15, 16, 17, and 18, corresponding to where demand is located. For the MV grid, all connection points are available. Costs of unitary energy capacity, power rating and fixed installation cost according to current market figures for Switzerland and are reported later when discussing results. Voltage statutory limits are 0.92 pu and 1.08 pu, line ampacity limits 0.8 pu, and the series resistance of the Thevenin equivalent circuit model of batteries is 0.01 pu and the same for all units.

[1] I.e., the surface of the installed capacity cannot exceed the geographical extension of the networks. Additionally, we place a cap on the size of each PV plant to achieve distributed PV generation. It is 70 MWp for the MV grid and 200 kWp for the LV.

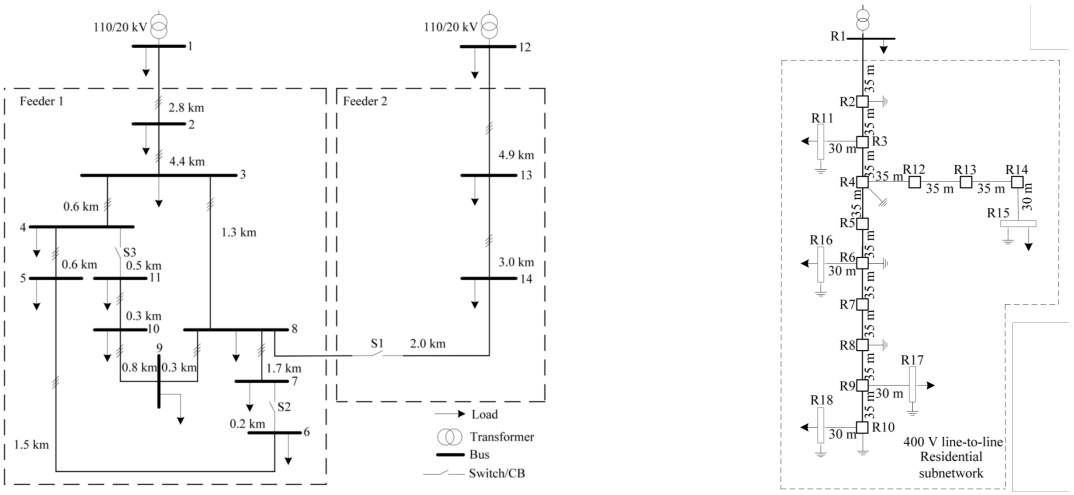

(a) . **(b)**

Figure 2: The two Cigre' benchmark electrical networks for medium voltage (a) and low voltage (b) [].

Table 1: Nominal demand and installed PV capacity per node for the MV and LV networks in the (base-case) scenario.

	Medium Voltage					Low Voltage		
Node	Residential		Commercial		PV Capacity	Residential		PV Capacity
	S[kVA]	pf	S[kVA]	pf	[kWp]	S[kVA]	pf	[kWp]
1	15300	0.98	5100	0.95	7000	200	0.95	200
2	–	–	–	–	6154	–	–	–
3	285	0.97	265	0.85	5380	–	–	–
4	445	0.97	–	–	2730	–	–	–
5	750	0.97	–	–	1570	–	–	–
6	565	0.97	–	–	110	–	–	–
7	–	–	90	0.85	–	–	–	–
8	605	0.97	–	–	–	–	–	–
9	–	–	675	0.85	1386	–	–	–
10	490	0.97	80	0.85	1988	–	–	–
11	340	0.97	–	–	7000	15	0.95	100
12	15300	0.98	5280	0.95	7000	–	–	–
13	–	–	40	0.85	–	–	–	–
14	215	0.97	390	0.85	618	–	–	–
15	NA	NA	NA	NA	NA	52	0.95	94
16	NA	NA	NA	NA	NA	55	0.95	99
17	NA	NA	NA	NA	NA	35	0.95	24
18	NA	NA	NA	NA	NA	47	0.95	–
Total	34295	–	11920	–	40936	404	–	517

Scenario of installed PV generation capacity PV installed capacity is expressed in percentage of the base case scenario reported in Table 1. For each network, we test 8 cases of installed PV capacity: from 0% to 300%, with 50% increments. For the LV network, we also test the 350% case.

Input time series As grid operational constraints are violated during events with large PV generation and low demand, we consider time series for periods of time with the largest level of PV production and lowest level of consumption. The time series of the active and reactive power demand, and PV generation are built from real measurements and shown in Fig. 3. These profiles are used to build the nodal injections by scaling and adapting them according to the nominal demand and power factor of each node. The PV production is determined with a physical modeling tool-chain, as described in [7], as a function of input global horizontal irradiance. We consider a fixed (non-tracking) PV installations with a configuration that maximizes PV generation at a Central European latitude, i.e., south facing and 41° tilt angle. The normalized demand and PV profile are shown in Fig. 3 with the time resolution of 1 hour. This profile is scaled as explained above

and use for all the nodes. In this way, we neglect smoothing effect due to spatial distribution and achieve a worse case representation of PV generation.

The PV generation pattern refers to a clear-sky day, which is generally conducive to the highest daily production values of PV, and it is indeed representative of the most optimistic scenario for PV generation production[2].

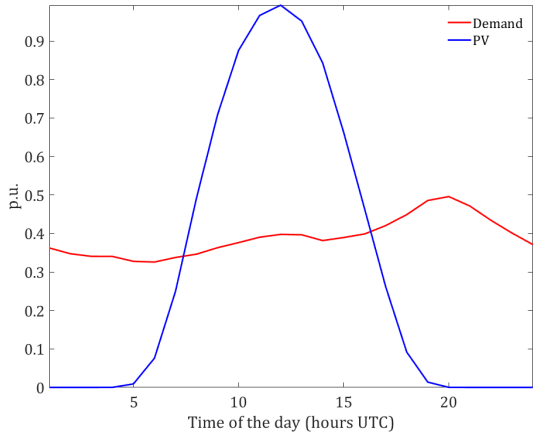

Figure 3: Normalized demand and PV profile.

3 Results and Discussion

3.1 Identified energy storage and power rating requirements

Low voltage grid Table 2 reports the energy storage capacity and the associated power rating to deploy in the LV network as a function of the PV installed capacity. Fig. 4a shows the total values of energy storage capacity and power rating for the whole network. Below the 100% scenario, which approximates the PV hosting capacity of the grid, there is no need for storage. In the 100% scenario, the amount of required storage is small, denoting that there are mild grid congestions to cope with. Above 100%, the need for storage capacity starts to increase nonlinearly, first, and linearly later, as further discussed in the next section. The node that is initially picked by the algorithm is node 15, a critical location at the end of a long feeder and in the proximity of a 55 kWp PV plant. For large values of installed PV generation capacity, nodes 11 and 15 are also selected.

Table 2: Identified power rating (kVA) and energy capacity (kWh) requirements at the nodes of the LV network.

PV scenario	0%		50%		100%		150%		200%		250%		300%	
Node	Power Rating	Energy Capac.	Power Rating	Energy Capac.	Power Rating	Energy Capac.	Power Rating	Energy Capac.	Power Rating	Energy Capac.	Power Rating	Energy Capac.	Power Rating	Energy Capac.
11	0	0	0	0	0	0	0	0	0	0	19.7	47.4	54	200
15	0	0	0	0	5.6	11	42.3	174.3	80.6	386	106	561	139	773
16	0	0	0	0	0	0	0	0	0	0	24.2	61.3	60	218
Total	0	0	0	0	5.6	11	42.3	174.3	80.6	386	149.9	669.7	253	1191

[2]It is worth noting that there might exist sky conditions, e.g., a broken sky day, that can determine local peaks of irradiance up to 15% larger than a clear-sky day due to the contribution of diffused irradiance. However, in such sky conditions, geographically sparse PV installations would not experience the peak at the same time due to spatial smoothing. Thus, it is reasonable to assume that the considered scenario is the most optimistic both from energy yield and instant power production perspective, and suitable to represent the most critical situation for distribution systems.

Medium voltage grid Results are reported in Table 3 and shown in Fig. 4b. Similarly to the previous case, a moderate amount of storage to cope with grid congestions is required in the 100% scenario. For increasing values of installed PV generation, the energy storage capacity and power rating requirements increase. The nodes which require storage are 11, 2 and 5.

Table 3: Identified power rating (MVA) and energy capacity (MWh) requirements at the nodes of the MV network.

PV scenario	0%		50%		100%		150%		200%		250%		300%	
Node	Power Rating	Energy Capac.	Power Rating	Energy Capac.	Power Rating	Energy Capac.	Power Rating	Energy Capac.	Power Rating	Energy Capac.	Power Rating	Energy Capac.	Power Rating	Energy Capac.
2	0	0	0	0	0	0	0	0	0	0	6.76	45.27	6.4	32.32
5	0	0	0	0	0	0	0	0	0	0	0	0	10.21	75
11	0	0	0	0	0.22	0.14	3.5	11.64	12.4	61.5	14.6	75	13.61	75
Total	0	0	0	0	0.22	0.14	3.5	11.64	12.4	61.5	21.36	120.27	30.22	182.32

The validation of the optimal power flow results is given in Appendix B.

3.2 Discussion

Relation between installed PV capacity and power rating of batteries For the LV network, Table 2 shows that, in the 200% case, the total power rating of the deployed battery systems is 80 kVA, much smaller than the increase in PV installed capacity, i.e., 500 kWp. In a network where the hosting capacity for generation is already saturated, one would expect that each additional kWp of generation should be adequately supported by an opposite amount of flexibility. However, it is to consider that PV generation is from distributed plants and that not all the additional PV capacity is conducive to overloading the network further. In particular, Table 1 shows that almost 300 kWp of installed PV capacity is connected at node 1 and 11, i.e., very close to the grid connection point. Unless there is a bottleneck in the transformer or a saturated line in the upper portion of the grid, additional PV capacity at these node is unlikely to determine violations of the voltage due to the short length of the cables. Fig. 4a shows that the power rating grows, first, non-linearly and, later, linearly with the installed PV capacity. The nonlinear trend can be explained by the nonlinear power flow equations and the fixed installation cost of batteries, which induce the algorithm to saturate the control potential and one node and oversize the power rating of already existing batteries before activating the placement of others. The linear trend can be explained by the fact that the hosting capacity of the nodes where PV generation is connected to is saturated and, thus, each additional kWp should be compensated by an opposite power rating capacity. This is also confirmed by the following observation. For the LV grid, the rate of growth of the power rating capacity is approx. 100 kW per 50% of the total installed PV capacity. However, if considering that 200 kWp is the generation capacity that congests the grid (because far away from the slack bus), the rate 100 kW/50% translates into 100 kW/100 kWp, denoting that each additional kWp should be compensated by an equal increase in the power rating from battery capacity. A similar consideration applies to the MV grid as well. As far as the trend of energy capacity is concerned, it is similar to the power rating, but it grows with a higher rate. The motivations for this are explained in the next paragraph.

C-rate of the battery fleet and relation power-energy The siting and sizing algorithm determines a battery fleet characterized by a total C-rate of about 0.15 hour^{-1} (i.e., the ratio between converter power rating and battery energy capacity), a small value compared to conventional design practices for grid-connected batteries, which generally refer to a range 1.5-2. On the one hand, the power rating of batteries is dictated by the peak value of PV generation, which requires a readily available capacity of apparent power to compensate for over-voltages and over-currents. On the other hand, the need for energy storage capacity depends on the duration of over-voltage and over-current events, or, in other words, on how much PV generation should be deferred and stored locally. The fact that the need for energy capacity grows faster than for power is to be expected since we are considering a PV production pattern of a spring clear-sky day (i.e., the worst-case scenario for electric grids) that delivers a consistent energy yield over an approximately

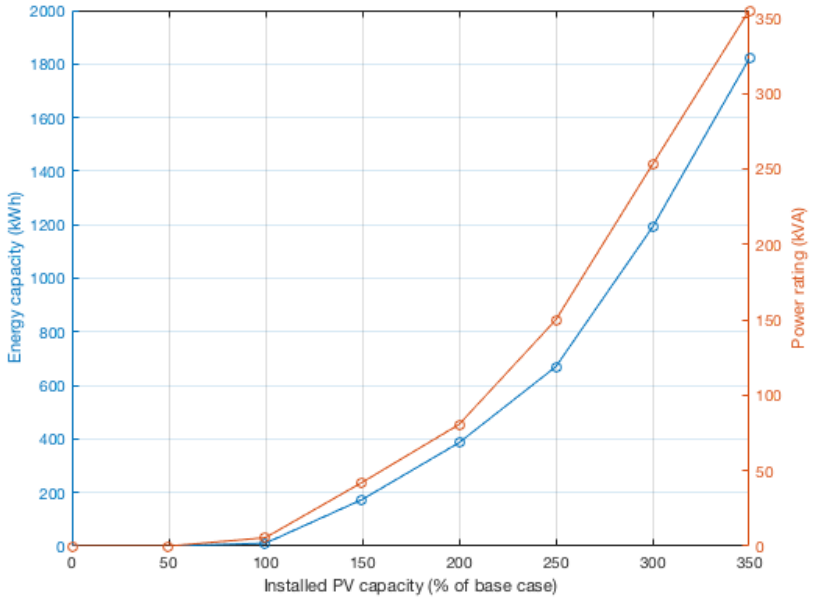

(a) LV grid.

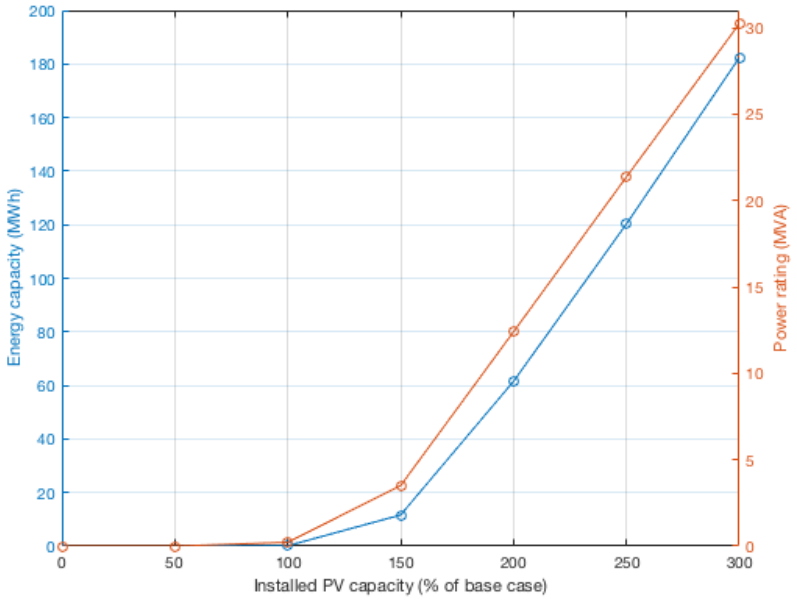

(b) MV grid.

Figure 4: Total energy storage capacity and converter power rating as a function of the installed PV capacity, where 100% denotes the approximated hosting capactiy of the grid.

8-hour period: if the PV injections determine an overload of the grid, power should be potentially stored locally for a long period to avoid violations of grid constraints. We can conclude that increasing the PV hosting capacity of distribution systems is an energy-intensive application. As grid-connected batteries are

typically designed with C-rate in the range 1.5-2, it can be efficiently coupled with power-intensive services (e.g., primary frequency control) by leveraging algorithms for stacking of ancillary services, e.g., [8], leading to a more efficient use of their potential.

3.3 Economic Evaluation

The costs considered in the analysis are according to current market figures. They are:

- unitary cost of power rating 1 200 CHF/kVA,
- unitary cost of energy capacity 400 CHF/kWh, and
- fixed installation cost 5 000 CHF for LV systems, 15 000 CHF for MV systems.

The capital costs to implement the storage deployment guidelines identified in the previous section are reported in Table 4. A comparison with the cost of conventional reinforcement strategies of distribution systems will be considered in future works. An alternative to deploying battery systems is curtailing PV generation. In this context, an economic trade-off between the capital costs for battery deployment and the operational costs of curtailing PV generation might exist and will be investigated in future works.

Table 4: Economical cost to implement identified storage deployment guidelines.

		PV						
Network	Unit	0%	50%	100%	150%	200%	250%	300%
LV	Kilo CHF	0	0	16	125	256	463	795
MV	Milion CHF	0	0	0.3	8.9	39.5	73.8	109.2

4 Conclusions

A method to determine the location, energy capacity and power rating of the batteries in electrical distribution systems to counterbalance grid congestions caused by excess PV generation was presented and applied to a LV and MV distribution network, modeled according to the specifications of the CIGRE's benchmark systems. The analysis was carried out for different levels of installed distributed PV generation capacity, from zero up to 3 times the generation hosting capacity of the grid. Uniform clear-sky conditions were considered as they are conducive to the largest yield from distributed PV generation and overloading the network. In the considered case studies, it is shown that for very large values of PV penetration levels (i.e., twice the PV hosting capacity), the total power rating of the deployed battery systems grows in a 1-to-1 ratio with the installed PV capacity. For less extreme values of installed PV capacity, the growth is generally smaller. The total energy capacity of batteries grows faster than for the power rating due to the typical peak production patterns of PV generation, that typically occur in the middle of the day and last for several hours. In particular, once the injection from a PV plant determines an over-current or over-voltage, it needs to be postponed and stored until it persists (e.g., hours) thus determining large energy capacity requirements. Using distributed battery storage to mitigate grid congestions caused by PV is an energy-intensive application that can be coupled with power-intensive applications, like primary frequency regulation, by leveraging algorithms for the provision of multiple ancillary services.

A Optimal power flow problem

The optimal power flow problem is a central component of many numerical procedures for power system planning and operation. Generally, it is a non-linear and non-convex problem due complicating multiplicative and trigonometric relationships. Solving it is computationally expensive and does not guarantee to find an optimal solution. A considerable research effort has been devoted in the recent literature to convexify and linearize efficiently the problem in order to make it tractable, e.g., [9–11]. An exact convex formulation of the optimal power flow problem was proposed in [11], considering also the transverse parameters of the network along with line ampacity and nodal voltage limits. The model relies on a complete transmission line two-port Π model.

B Verification of optimal power results

We verify whether the representation of voltage and current constraints in the optimal power flow problem at the previous step are respected by playing its output (i.e., nodal injections) back in a load flow problem. Fig. 5a shows, in the upper panel, the values of the line currents in the optimal power flow model and load flow problem and, in the lower panel, their difference. Fig. 5b shows, in the upper panel, the values of the nodal voltages in the optimal power flow model and load flow problem and, in the lower panel, their difference. Values do not report any constraint violation. Statistics on the residuals of nodal voltages and line currents are shown in Table 5, and denote negligible errors due to numerical approximations of the solver. This is as expected, since the adopted optimal power flow formulation leverages an exact representation of load flow equations.

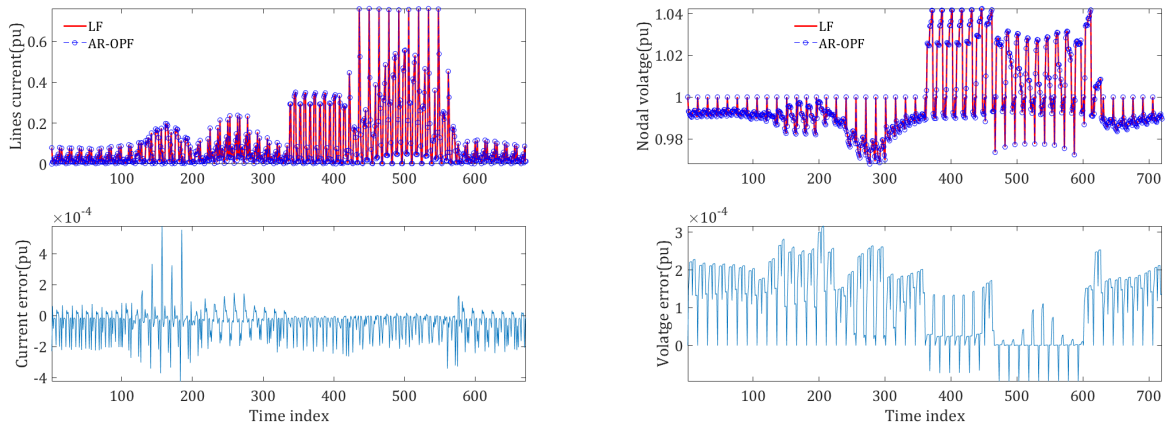

(a) Line currents. **(b)** Nodal voltages.

Figure 5: Comparison of the optimal power flow's output against a load flow analysis subject to the same nodal injections.

Table 5: Statistics on performances of AR-OPF.

Quantities	RMSE	Mean	Max
Voltage (pu)	1.51e-4	1.17e-4	3.16e-4
Current (pu)	1.06e-4	-4.7e-5	5.79e-4

References

[1] M. Nick, R. Cherkaoui, and M. Paolone, "Optimal planning of distributed energy storage systems in active distribution networks embedding grid reconfiguration," *IEEE Transactions on Power Systems*, vol. 33, no. 2, pp. 1577–1590, 2018.

[2] E. Stai, L. Reyes, F. Sossan, J.-Y. Le Boudec, and M. Paolone, "Dispatching stochastic heterogeneous resources accounting for grid losses and imperfect batteries," *IEEE Transactions on Smart Grid*, vol. (Accepted for publication, available online, 2017.

[3] M. Kraning, Y. Wang, E. Akuiyibo, and S. Boyd, "Operation and configuration of a storage portfolio via convex optimization," in *Proceedings of the 18th IFAC World Congress*, vol. 18. Citeseer, 2011, pp. 10 487–10 492.

[4] E. Namor, D. Torregrossa, F. Sossan, R. Cherkaoui, and M. Paolone, "Assessment of battery ageing and implementation of an ageing aware control strategy for a load leveling application of a lithium titanate battery energy storage system," in *2016 IEEE 17th Workshop on Control and Modeling for Power Electronics (COMPEL)*, June 2016.

[5] C. T. F. C6.04.02, "Benchmark systems for network integration of renewable and distributed energy resources," Cigre' International Council on large electric systems, Tech. Rep., July 2009.

[6] F. Sossan, J. Darulova, M. Paolone, A. Kahl, S. J. Bartlett, and M. Lehning, "Large scale deployment of pv units in existing distribution networks: Optimization of the installation layout," in *2016 Power Systems Computation Conference (PSCC)*, June 2016.

[7] E. Scolari, F. Sossan, and M. Paolone, "Photovoltaic model-based solar irradiance estimators: Performance comparison and application to maximum power forecasting," *IEEE Transactions on Sustainable Energy*, 2017.

[8] E. Namor, F. Sossan, R. Cherkaoui, and M. Paolone, "Control of battery storage systems for the simultaneous provision of multiple services," *IEEE Transactions on Smart Grid*, pp. 1–1, 2018.

[9] L. Gan, N. Li, U. Topcu, and S. Low, "On the exactness of convex relaxation for optimal power flow in tree networks," in *Decision and Control (CDC), 2012 IEEE 51st Annual Conference on*. IEEE, 2012, pp. 465–471.

[10] L. Gan, N. Li, U. Topcu, and S. H. Low, "Exact convex relaxation of optimal power flow in radial networks," *IEEE Transactions on Automatic Control*, vol. 60, no. 1, pp. 72–87, 2015.

[11] M. Nick, R. Cherkaoui, J.-Y. Le Boudec, and M. Paolone, "An exact convex formulation of the optimal power flow in radial distribution networks including transverse components," *IEEE Transactions on Automatic Control*, vol. 63, no. 3, pp. 682–697, 2018.